International Journal of Fracture **117:** 347–358, 2002.

Numerical modeling of size effects with gradient elasticity - Formulation, meshless discretization and examples

HARM ASKES* and ELIAS C. AIFANTIS†‡
**Delft University of Technology, Faculty of Civil Engineering and Geosciences, P.O. Box 5048, 2600 GA Delft, Netherlands;*
†Aristotle University of Thessaloniki, Polytechnic School, Laboratory of Mechanics and Materials, 54006 Thessaloniki, Greece;
‡Michigan Technological University, Center for Mechanics of Materials and Instabilities, Houghton, MI49931, USA

Received 15 June 2001; accepted in revised form 26 Augustus 2002

Abstract. A theory of gradient elasticity is used and numerically implemented by a meshless method to model size effects. Two different formulations of this model are considered, whereby the higher-order gradients are incorporated explicitly and implicitly, respectively. It turns out that the explicit gradient dependence leads to a straightforward spatial discretization, while use of the implicit gradient dependence can result in an awkward form of the stiffness matrix. For the numerical analyses the Element-Free Galerkin method has been used, due to its ability to incorporate higher-order gradients in a straightforward manner. Two boundary value problems have been considered, which show the capability of the gradient elasticity theory to capture size effects. In a follow-up paper, the formulation developed herein will be used to analyze additional configurations with attention to comparison with available experimental data on size effects and verification of available scaling laws for structural components.

Key words: gradient elasticity, size effect, Element-Free Galerkin method, higher-order continuum

1. Introduction

The size effect is currently a subject of increasing interest. The existence of a size effect implies that different specimens with similar geometries but different dimensions expose a different mechanical behavior. The size effect is normally quantified by considering the so-called 'nominal strength', which is typically defined as the applied load divided by a characteristic cross-sectional area of the specimen. Size effects have been noted for a range of materials including concrete (Bažant, 1984, 2000; Carpinteri et al., 1995; Van Vliet, 2000), soils (Vardoulakis and Sulem, 1995), metals (Fleck et al., 1994) and composites (Zhu et al., 1997). From the point of view of material modeling, it is crucial that the employed material model can capture size effects adequately when this is necessary. An overview of size effect phenomena in material modeling can be found in (Carpinteri, 1996).

It is well established that classical linear elastic continua, in which the stresses depend only on the strains and no higher-order terms are involved, are not able to describe size effects. These continua lack an internal length scale. In contrast, enhanced continua such as appear in nonlocal or gradient-dependent models do possess an internal length scale. Through this length scale, which enters the model as an additional material parameter, size effects can be modeled properly. This has first been illustrated explicitly in (Aifantis, 1996) through the use of a simple gradient elasticity model to solve the 'borehole' boundary value problem.

The analytical solution contained the ratio of the internal length parameter to the size of the hole, and the influence of this ratio was diminishing for large holes. It was also shown that smaller holes are stronger. In the same article, simple gradient elasticity and plasticity models were incorporated within a strength of materials approach to interpret size effects in elastic and plastic torsion and bending (Fleck et al., 1994; Lakes, 1983, 1986, Morrison, 1939; Richards, 1958). To this end, the solution of the boundary-value problem was not required, even though this was the case in a related work (Zhu et al., 1997) where size effects in metal-matrix composites were captured by incorporating a deformation model of gradient plasticity within a unit cell numerical formulation. Numerical solution of boundary-value problems is also required for other internal length approaches such as nonlocal models (Pijaudier-Cabot et al., 1987) which have been used to capture size effects in fracture.

As mentioned above, in a previous contribution by Aifantis (1999b), size effects as envisaged in gradient elasticity and gradient plasticity theories have been discussed within a simple mechanics of materials formulation. For approximate, one-dimensional cases of torsion and bending analytical expressions have been found in gradient elasticity and gradient plasticity that, upon fitting the constitutive parameters, give excellent correlations with experimentally obtained size effects. The current contribution aims at extending the gradient approach to size effects through the solution of related boundary value problems for more general geometric configurations. To this end, a numerical approach is taken. The gradient elasticity theory as proposed in (Aifantis, 1999a, b; Altan and Aifantis, 1997) has been discretized using the Element-Free Galerkin (EFG) method (Belytschko et al., 1994; 1996, Lu et al., 1994). The motivation for using the EFG method is that EFG shape functions are easily formulated with any desired order of continuity. Thus, higher-order gradients can be incorporated into the model without the need of Hermitian formulations, which makes the EFG method a suitable tool for testing the performance of higher-order gradient models (Askes, 2000; Askes et al., 2000; Pamin et al., 1999).

First, the governing equations of gradient elasticity are reviewed. A distinction is made between the original formulation as proposed by Aifantis on the one hand, and a modified formulation that follows the work of Peerlings and co-workers in gradient-enhanced damage formulations (Peerlings et al., 1996a, 1996b, 1998). Next, the spatial discretization of the two formulations is treated. Two examples are presented: a cantilever beam and a square plate with a hole under uniaxial tension.

Throughout, matrix-vector notation is used.

In concluding this outline, it is noted that additional configurations have been worked out, including perforated strips under tension, notched beams under bending and indentation problems. This allows for comparison of the size effect results predicted by gradient elasticity with corresponding experimental data available in the literature. Moreover, it allows for a direct verification of various scaling laws (Bažant, 2000; Carpinteri et al., 1995) that have been proposed to generically describe the size effect behavior of structural components. These issues will be included in a follow-up of the present work.

2. Gradient elasticity formulations

The addition of higher-order strain gradients provides a successful and simple means of enhancing some of the disadvantageous properties of a classical continuum formulation. For instance, singularities in the strain field near crack tips can be removed by using a continuum

elasticity formulation in which the stresses do not depend only on the strains, but also on the second derivatives thereof (Altan et al., 1992, 1997). Similarly, the addition of higher-order gradients of the state variables has been shown to be effective in maintaining well-posedness of the mathematical description in strain-softening problems with plasticity or damage formulations, (e.g., de Borst and Mülhaus, 1992; Mülhaus and Aifantis, 1991; Peerlings et al., 1996a, b). The higher-order gradients reflect the influence of the underlying heterogeneous microstructure upon the stress-strain law. In this way, microstructural properties which are essential to describe scale-dependent macroscopic phenomena are taken into account in a physically realistic manner.

In the simplest form of gradient elasticity theory proposed by Aifantis the classical stress-strain relation is augmented by a second-order strain gradient as

$$\boldsymbol{\sigma} = \mathbf{D}(\boldsymbol{\varepsilon} - l^2\nabla^2\boldsymbol{\varepsilon}) \tag{1}$$

in which $\boldsymbol{\sigma}$ and $\boldsymbol{\varepsilon}$ contain the components of stress and strain, respectively, $\mathbf{D}$ contains the elastic moduli and l is a material parameter with the dimension of length related to the microstructure. The classical continuum is retrieved by setting $l = 0$.

In Equation (1), the higher-order term is preceded by a negative sign. It can be shown that this is essential in order to guarantee uniqueness of the boundary-value problem (Altan and Aifantis, 1997). On the other hand, for a closer approximation of the dispersive properties of a discrete medium in wave propagation problems, a positive sign in front of the higher-order term is more desirable. However, a positive sign leads to a model for which uniqueness cannot be guaranteed (Altan and Aifantis, 1997) and for which totally unrealistic results are obtained in static (Askes et al., 2002) as well as dynamic analysis (Askes et al., 2001b, 2002). For dynamical problems a proper combination of higher-order stiffness and higher-order inertia terms may resolve simultaneously the above difficulties (Askes and Metrikine, 2002; Metrikine and Askes, 2002). In this connection, it is noted that more elaborate gradient elasticity formulations exist. For instance, also nonlinear gradient terms (Aifantis, 1999b) or fourth-order gradients can be included (Askes et al., 2001a, 2002). It has been shown that the combination of a second-order gradient and a fourth-order gradient leads to an improved performance in wave propagation problems as compared to the model of Equation (1), see (Askes et al., 2001b, 2002. Conversely, the behavior of the fourth-order model is similar to that of the second-order model of Equation (1) for static analyses. As such, for the purpose of the present contribution in which only static cases are considered it suffices to investigate the simple form as given in Equation (1).

Equation (1) can equally be written as

$$\boldsymbol{\sigma} = \mathbf{D}\tilde{\boldsymbol{\varepsilon}} \tag{2}$$

where

$$\tilde{\boldsymbol{\varepsilon}} = \boldsymbol{\varepsilon} - l^2\nabla^2\boldsymbol{\varepsilon} \tag{3}$$

In fact, formulation (3) can be considered as a series approximation of an integral expression (which has been truncated after the second-order term) for the average (nonlocal) strains $\tilde{\boldsymbol{\varepsilon}}$ in terms of the local strains $\boldsymbol{\varepsilon}$. This average is then taken over a finite material volume which is defined by the internal length. In Equation (3), the non-standard strain vector $\tilde{\boldsymbol{\varepsilon}}$ is related to the standard strain vector $\boldsymbol{\varepsilon}$ in an *explicit* manner. As an alternative, it has been proposed to rewrite Equation (3) in order to give an *implicit* relation between $\tilde{\boldsymbol{\varepsilon}}$ and $\boldsymbol{\varepsilon}$. Accordingly,

the second derivative of $\tilde{\boldsymbol{\varepsilon}}$ in Equation (3) is taken and multiplied by l^2 (Askes et al., 2000; Peerlings et al., 1996a, b; Peerlings et al., 1998), i.e.

$$l^2\nabla^2\tilde{\boldsymbol{\varepsilon}} = l^2\nabla^2\boldsymbol{\varepsilon} - l^4\nabla^4\boldsymbol{\varepsilon} \tag{4}$$

Next, Equation (4) is back-substituted into Equation (3). When the fourth-order term is neglected, the result reads

$$\tilde{\boldsymbol{\varepsilon}} + l^2\nabla^2\tilde{\boldsymbol{\varepsilon}} = \boldsymbol{\varepsilon} \tag{5}$$

Alternatively, this result can be obtained by writing Equation (3) in operator form (see for instance earlier work of Aifantis and coworkers (Altan and Aifantis, 1992; Ru and Aifantis, 1993)), that is $\tilde{\boldsymbol{\varepsilon}} = (1 - l^2\nabla^2)\boldsymbol{\varepsilon}$. Thus,

$$\boldsymbol{\varepsilon} = \frac{1}{1 - l^2\nabla^2}\tilde{\boldsymbol{\varepsilon}} \approx (1 + l^2\nabla^2)\tilde{\boldsymbol{\varepsilon}} \tag{6}$$

where a Taylor's first term approximation was used under the assumption that $l^2\nabla^2 \ll 1$. The difference between Equations (3) and (5) only concerns the gradient term, either in terms of $\boldsymbol{\varepsilon}$ or in terms of $\tilde{\boldsymbol{\varepsilon}}$. In the sequel, the original equation (1) will be referred to as the *explicit* formulation, whereas the combination of Equations (2) and (5) is denoted as the *implicit* formulation. The advantages of using an implicit formulation instead of an explicit formulation have been reported in the literature on gradient-enhanced damage models. For instance, lower continuity requirements are put on the shape functions in case of a numerical approach (Askes, 2000; Peerlings et al., 1996a), the dynamical behaviour is more realistic (Peerlings et al., 1996b), a better approximation of the underlying nonlocal integral model is given (Askes et al., 2000; Peerlings et al., 1996b) and singularities in the strain field are damped more adequately (Peerlings, 1999).

3. Spatial discretization

In order to carry out numerical analyses, the gradient elasticity equations must be discretized in conjunction with the equilibrium equations and the kinematic relations. The Element-Free Galerkin (EFG) method is used for this purpose, the shape functions for which are treated briefly.

3.1. Explicit formulation

The starting point is the weak formulation of the equilibrium equation

$$\int_\Omega \delta\mathbf{u}^T(\mathbf{L}^T\boldsymbol{\sigma} + \mathbf{b})\mathrm{d}\Omega = 0 \tag{7}$$

in which $\delta\mathbf{u}$ contains the virtual displacements that correspond to the stress field $\boldsymbol{\sigma}$, $\mathbf{b}$ contains the body forces, and $\mathbf{L}$ is the differential operator:

$$\mathbf{L}^T = \begin{bmatrix} \dfrac{\partial}{\partial x} & 0 & 0 & \dfrac{\partial}{\partial y} & 0 & \dfrac{\partial}{\partial z} \\ 0 & \dfrac{\partial}{\partial y} & 0 & \dfrac{\partial}{\partial x} & \dfrac{\partial}{\partial z} & 0 \\ 0 & 0 & \dfrac{\partial}{\partial z} & 0 & \dfrac{\partial}{\partial y} & \dfrac{\partial}{\partial x} \end{bmatrix} \tag{8}$$

Integrating the stress term by parts yields

$$\int_\Omega \delta\boldsymbol{\varepsilon}^T\boldsymbol{\sigma}\,\mathrm{d}\Omega = \int_\Omega \delta\mathbf{u}^T\mathbf{b}\mathrm{d}\Omega + \int_{\Gamma_t} \delta\mathbf{u}^T\mathbf{t}\mathrm{d}\Gamma \tag{9}$$

with $\mathbf{t}$ the prescribed tractions on the free part of the boundary Γ_t, and $\boldsymbol{\varepsilon} = \mathbf{L}\mathbf{u}$. Next, the constitutive equation (1) is substituted, and the higher-order term is again integrated by parts. Thus,

$$\int_\Omega \delta\boldsymbol{\varepsilon}^T\mathbf{D}\boldsymbol{\varepsilon}\mathrm{d}\Omega + \int_\Omega \frac{\partial\delta\boldsymbol{\varepsilon}^T}{\partial\xi}\mathbf{D}l^2\frac{\partial\boldsymbol{\varepsilon}}{\partial\xi}\mathrm{d}\Omega = \int_\Omega \delta\mathbf{u}^T\mathbf{b}\mathrm{d}\Omega + \int_{\Gamma_t} \delta\mathbf{u}^T\mathbf{t}\mathrm{d}\Gamma + \oint_\Gamma \delta\boldsymbol{\varepsilon}^T\mathbf{D}l^2\frac{\partial\boldsymbol{\varepsilon}}{\partial\xi}\mathrm{d}\Gamma \tag{10}$$

where a summation over $\xi = x_1, x_2, x_3$ is implied. Due to the higher-order terms that have appeared in the constitutive relation, also higher-order boundary conditions are needed. Here, it is assumed that the derivatives of $\boldsymbol{\varepsilon}$ vanish on the boundary. Hence, the last boundary integral in Equation (10) cancels.

Discretizing the test and trial functions via $\delta\mathbf{u}^T = \delta\underline{\mathbf{u}}^T\mathbf{H}^T$ and $\mathbf{u} = \mathbf{H}\underline{\mathbf{u}}$, and requiring that Equation (10) holds for any admissible $\delta\underline{\mathbf{u}}$ leads to

$$[\mathbf{K}_0 + \mathbf{K}_1]\underline{\mathbf{u}} = \mathbf{f}^{\mathrm{ext}} \tag{11}$$

in which the standard stiffness matrix $\mathbf{K}_0$ is given by

$$\mathbf{K}_0 = \int_\Omega \mathbf{B}^T\mathbf{D}\mathbf{B}\mathrm{d}\Omega \tag{12}$$

with $\mathbf{B} = \mathbf{L}\mathbf{H}$, the higher-order stiffness matrix $\mathbf{K}_1$ reads

$$\mathbf{K}_1 = \int_\Omega \frac{\partial\mathbf{B}^T}{\partial\xi}\mathbf{D}l^2\frac{\partial\mathbf{B}}{\partial\xi}\mathrm{d}\Omega \quad \xi = x_1, x_2, x_3 \tag{13}$$

and the external force vector $\mathbf{f}^{\mathrm{ext}}$ is given by

$$\mathbf{f}^{\mathrm{ext}} = \int_\Omega \mathbf{H}^T\mathrm{d}\mathrm{d}\Omega + \int_{\Gamma_t} \mathbf{H}^T\mathbf{t}\mathrm{d}\Gamma \tag{14}$$

From Equation (11) it can be seen that the only difference with a classical continuum model concerns the higher-order stiffness matrix. For this term, second (rather than first) derivatives of the shape functions have to be computed. Furthermore, the shape functions need to be $\mathcal{C}^1$ continuous (cf., the discretization of the Timoshenko beam theory). This poses no problems in case EFG shape functions are used. However, in a finite element context Hermitian formulations (Pamin, 1994) or other modifications (Amanatidou and Avras, 2002) are necessary.

3.2. Implicit formulation

In the implicit formulation, Equations (2) and (5) have to be solved simultaneously with the equilibrium equation and the kinematic relation. Since the non-standard strain $\tilde{\boldsymbol{\varepsilon}}$ appears as an independent unknown in the differential equations, it is discretized separately (Askes, 2000; Askes et al., 2000; Peerlings et al., 1996a, 1998). Substituting Equation (2) into Equation (9) yields

$$\int_\Omega \delta\boldsymbol{\varepsilon}^T\mathbf{D}\tilde{\boldsymbol{\varepsilon}}\mathrm{d}\Omega = \int_\Omega \delta\mathbf{u}^T\mathbf{b}\mathrm{d}\Omega + \int_{\Gamma_t} \delta\mathbf{u}^T\mathbf{t}\mathrm{d}\Gamma \tag{15}$$

The weak form of Equation (5) can be written as

$$\int_\Omega \delta\tilde{\boldsymbol{\varepsilon}}^T(\tilde{\boldsymbol{\varepsilon}} + l^2\nabla^2\tilde{\boldsymbol{\varepsilon}} - \boldsymbol{\varepsilon})\mathrm{d}\Omega = 0 \tag{16}$$

in which $\delta\tilde{\boldsymbol{\varepsilon}}$ is the test function that corresponds to $\tilde{\boldsymbol{\varepsilon}}$. Integrating the higher-order term by parts yields

$$\int_\Omega \delta\tilde{\boldsymbol{\varepsilon}}^T(\tilde{\boldsymbol{\varepsilon}} - \boldsymbol{\varepsilon})\mathrm{d}\Omega - \int_\Omega \frac{\partial\delta\tilde{\boldsymbol{\varepsilon}}^T}{\partial\xi} l^2 \frac{\partial\tilde{\boldsymbol{\varepsilon}}}{\partial\xi}\mathrm{d}\Omega = 0 \tag{17}$$

where again a summation over $\xi = x_1, x_2, x_3$ is performed, and where vanishing derivatives of $\tilde{\boldsymbol{\varepsilon}}$ are taken for the higher-order boundary conditions.

Discretization is performed using shape functions $\mathbf{H}$ for the test and trial functions of the displacements and shape functions $\mathbf{N}$ for the test and trial functions of the non-standard strains. Thus,

$$\begin{bmatrix} \mathbf{K}_{uu} & \mathbf{K}_{u\varepsilon} \\ \mathbf{K}_{\varepsilon u} & \mathbf{K}_{\varepsilon\varepsilon} \end{bmatrix} \begin{bmatrix} \underline{\mathbf{u}} \\ \underline{\tilde{\boldsymbol{\varepsilon}}} \end{bmatrix} = \begin{bmatrix} \mathbf{f}^{\mathrm{ext}} \\ \mathbf{0} \end{bmatrix} \tag{18}$$

where $\underline{\tilde{\boldsymbol{\varepsilon}}}$ contains the discretized values of $\tilde{\boldsymbol{\varepsilon}}$, and

$$\mathbf{K}_{uu} = \mathbf{0} \tag{19}$$

$$\mathbf{K}_{u\varepsilon} = \int_\Omega \mathbf{B}^T\mathbf{D}\mathbf{N}\mathrm{d}\Omega \tag{20}$$

$$\mathbf{K}_{\varepsilon u} = \int_\Omega \mathbf{N}^T\mathbf{B}\mathrm{d}\Omega \tag{21}$$

$$\mathbf{K}_{\varepsilon\varepsilon} = \int_\Omega \mathbf{N}^T\mathbf{N}\mathrm{d}\Omega - \int_\Omega \frac{\partial\mathbf{N}^T}{\partial\xi} l^2 \frac{\partial\mathbf{N}}{\partial\xi}\mathrm{d}\Omega \quad \xi = x_1, x_2, x_3 \tag{22}$$

In contrast to system (11), system (18) has an awkward structure. This becomes manifest in three ways:

1. The zero block that forms $\mathbf{K}_{uu}$ destroys the positive definiteness of the system. This is a drawback, but not prohibitve.
2. In combination with Lagrange multipliers for the imposition of essential boundary conditions, it is possible that the total matrix in Equation (18) becomes rank-deficient. In that case, another zero block enters the global stiffness matrix on the diagonal, which can preclude the solution of Equation (18), see (Zienkiewicz et al., 1989).
3. Compared to system (11), the number of unknowns has increased by 150% in 2D and even 200% in 3D due to the relative length of $\tilde{\boldsymbol{\varepsilon}}$ as compared to $\mathbf{u}$. This puts enormous demands on the computer resources for large-scale simulations.

From a numerical point of view there is no added value using the implicit formulation instead of the explicit formulation. It has to be concluded that the present form of implicit gradient elasticity is unsuitable for use in a numerical context. Attempts to overcome these deficiencies are beyond the scope of the present study.

Remark *In the present form, system (18) is non-symmetric. If a symmetric system is desired, Equation (5) can be pre-multiplied by* **D***, after which discretization results in a symmetric system.*

3.3. Element-Free Galerkin shape functions

Below, the formulation of the Element-Free Galerkin (EFG) shape functions is discussed briefly. More details can be found in References (Belytschko et al., 1994, 1996; Lu et al., 1994).

In the EFG method only nodes and no elements are used to formulate the shape functions. Each node is assigned a so-called domain of influence in which its shape function is non-zero. This domain of influence is set through a so-called weight function $w(s)$. In this study a circular domain of influence with radius d is taken as

$$w(s) = \begin{cases} \dfrac{\exp\left(-\dfrac{s^2}{(\alpha d)^2}\right) - \exp\left(-\dfrac{d^2}{(\alpha d)^2}\right)}{1 - \exp\left(-\dfrac{d^2}{(\alpha d)^2}\right)} & \text{if } s \leq d \\ 0 & \text{if } s > d \end{cases} \tag{23}$$

with $s = |x - x_i|$ and α a numerical parameter to set the relative weights inside the domain of influence. Here, $\alpha = 1/4$. A polynomial base vector $\mathbf{p}$ is defined for one spatial dimension as, e.g.,

$$\mathbf{p}^T = [1, x, x^2, x^3, \dots] \tag{24}$$

The approximant function u^h is expressed in terms of EFG shape functions ϕ and nodal parameters $\mathbf{u}$ as

$$u^h = \phi^T \mathbf{u} \tag{25}$$

where

$$\phi^T = \mathbf{p}^T \mathbf{A}^{-1} \mathbf{C} \tag{26}$$

and

$$\mathbf{A} = \sum_{i=1}^{n} w_i \mathbf{p}_{(x_i)} \mathbf{p}_{(x_i)}^T \tag{27}$$

$$\mathbf{C} = [w_1 \mathbf{p}_{(x_1)}, w_2 \mathbf{p}_{(x_2)}, \dots, w_n \mathbf{p}_{(x_n)}] \tag{28}$$

in which n is the number of nodes and $wi_i = w(x - x_i)$. The matrices $\mathbf{B}$, $\mathbf{H}$ and $\mathbf{N}$ in Equations (11) and (18) contain the shape functions ϕ ordered with respect to the number of nodes and the number of spatial dimensions.

The relevant parameters that determine the quality of the EFG discretization are the radius of the domain of influence d, the nodal spacing denoted here with h, and the number of terms that are contained in the polynomial base vector $\mathbf{p}$. For the shape functions of the displacements a complete cubic polynomial base vector $\mathbf{p}$ and $d/h = 6$ are taken, while for the Lagrange multipliers that have been used a complete quadratic base vector and $d/h = 5$ are applied.

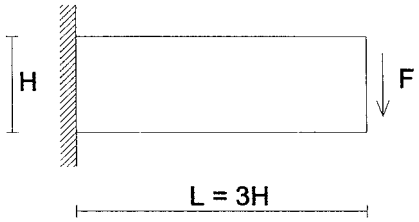

Figure 1. Clamped beam – geometry and loading conditions

4. Numerical examples

For the following numerical examples a plane strain assumption is adopted. A unit thickness of the specimen is also assumed.

4.1. Clamped beam under bending loading

The first example concerns a cantilever beam clamped on one end and with an applied force on the other end. The geometry and loading conditions are given in Figure 1. The beam height is denoted by H. A Poisson's ratio $\nu = 0.25$ is taken. The numerical discretization consists of 7×19 nodes, while each quadrilateral between 4 nodes is subdivided into 4×4 integration cells.

For this example, the ratio of the maximum bending strain ε_{cbt} (as predicted by the classical beam theory) and maximum bending strain ε_{num} (as predicted by the numerical model) is considered. Obviously, the classical beam theory does not contain any internal length parameter, and it is not able to model size effects. According to classical beam theory (Gere et al., 1991), the curvature κ near the clamped end is

$$\kappa = \frac{FL}{\frac{1}{12}EH^3} \tag{29}$$

so that

$$\varepsilon_{\text{cbt}} = \frac{1}{2}H\kappa = \frac{6F\alpha}{EH} \tag{30}$$

Thus,

$$\text{strain ratio} = \frac{6F\alpha/EH}{\varepsilon_{\text{num}}} \tag{31}$$

where α is the beam length-to-height ratio, which equals 3 in this case. A stiffness ratio of the specimen is defined in a similar manner as

$$\text{stiffness ratio} = \frac{E/4\alpha^3}{F/u_{\text{tip}}} \tag{32}$$

in which u_{tip} is the tip deflection as given by the numerical model, and where $E/4\alpha^3$ is the stiffness as predicted by the classical beam theory. With these definitions of strain ratio and stiffness ratio, values approximating one are obtained if the internal length parameter is neglible compared to the geometric dimensions of the specimen. On the other hand, if the internal length parameter becomes of significant magnitude, the peak strain and the tip

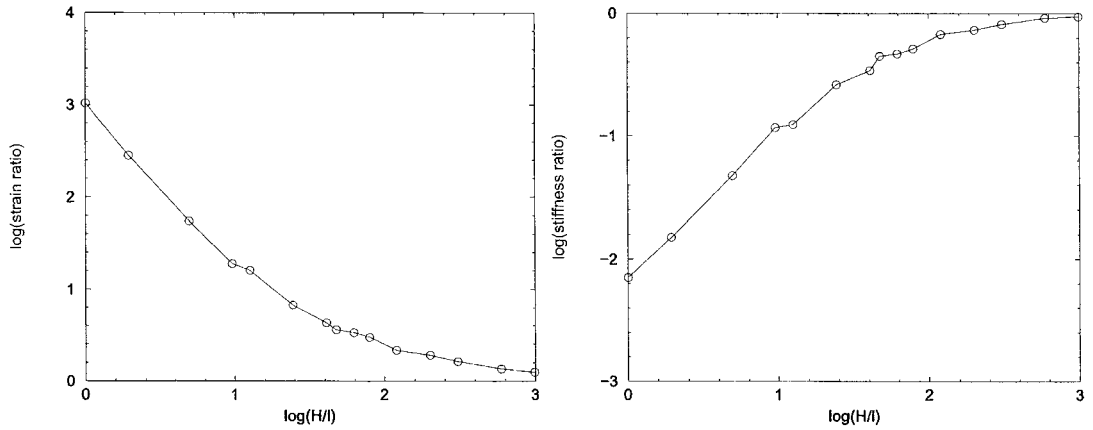

Figure 2. Clamped beam – size effect for strain ratio (left) and stiffness ratio (right)

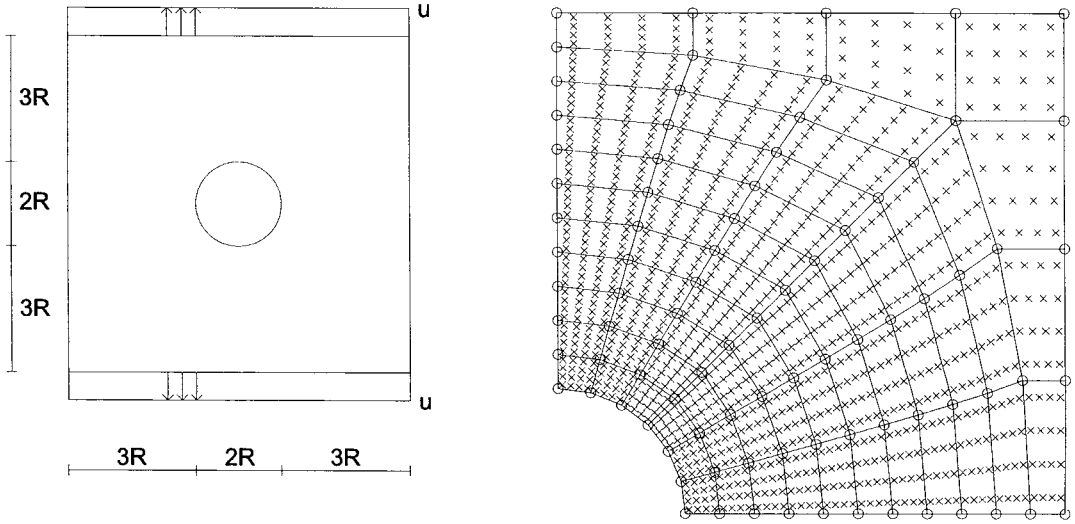

Figure 3. Square with hole – geometry and loading conditions (left) and EFG discretization of upper right quarter with nodes ∘ and integration points × (right)

displacement as predicted by the numerical model will decrease, so that the strain ratio will increase and the stiffness ratio will decrease.

The logarithm of strain ratio and stiffness ratio are plotted as a function of the logarithm of the normalized beam height H/l in Figure 2. Clearly, for increasing values of H/l the strain ratio increases and the stiffness ratio decreases. The higher-order gradient that has entered the constitutive equation smooths the strain field, such that the peak strain is lowered (which results in an increased strain ratio) and the stresses are redistributed (which results in a decreased stiffness ratio).

4.2. SQUARE WITH HOLE UNDER UNIAXIAL TENSION

As a second example, a square plate with a centric circular hole is considered. Figure 3 shows the geometry, loading conditions and the EFG discretization. For reasons of symmetry, only one quarter of the plate is modeled. Again, $\nu = 0.25$. Here, the strain ratio is defined as the

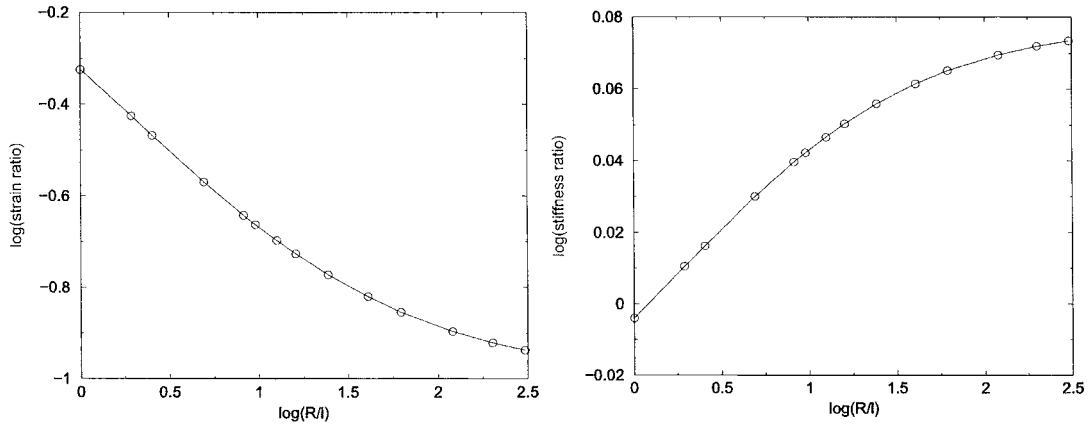

Figure 4. Square with hole – size effect for strain ratio (left) and stiffness ratio (right)

ratio of average strain over maximum strain as provided by the numerical solution, whereby the average strain is taken as the ratio of the imposed displacement over half the specimen length. That is,

$$\text{strain ratio} = \frac{u_{\text{imposed}}/4R}{\varepsilon_{\max}} \tag{33}$$

where $\varepsilon_{\max}$ is computed in the integration point directly right of the hole (see Figure 3). Indeed, this value is directly related to the stress intensity factor as it is predicted by the numerical model. For the stiffness ratio it is taken simply that

$$\text{stiffness ratio} = \frac{F_{\text{reaction}}/u_{\text{imposed}}}{E} \tag{34}$$

with F_{reaction} the reaction force applied at either end of the plate. For increasing values of the internal length parameter the maximum strain in the numerical model will decrease while the reaction force will increase, so that the strain ratio will increase and the stiffness ratio will decrease.

Figure 4 shows the strain ratio and stiffness ratio as a function of the normalized hole radius R/l, again with logarithmic scales. Note that for $R/l \to \infty$ the strain ratio curve reaches the value of $\log\left(\frac{1}{3}\right) \approx -1.1$, since the strain intensity factor of the classical continuum is 3.

5. Conclusions

In this paper, size effects in gradient elasticity models have been studied. By means of numerical two-dimensional examples it is established that the gradient elasticity model as proposed by Aifantis is capable of describing size effects. As such, this paper is an extension of earlier, one-dimensional investigations of size effects in gradient elasticity models.

Two different formulations of gradient elasticity have been considered. The original, so-called *explicit* formulation leads to a straightforward discretization. On the other hand, the alternative *implicit* formulation gives some numerical anomalies. It is concluded that the implicit formulation is not suitable for the present gradient elasticity framework.

For the numerical examples the Element-Free Galerkin (EFG) method has been applied. Due to the high order of continuity of the EFG shape functions, incorporation of higher-order

gradients is simple. In a follow-up paper, perforated tensile strips and notched three-point bending specimens will be considered to further illustrate EFG simulations of gradient models, along with some standard indentation configurations. The emphasis here will be on the comparison of the gradient elasticity size effect predictions with available experimental data for these test configurations, as well as on the possible verification of recently proposed scaling laws for structural components (Bažant, 2000; Carpinteri et al., 1995; Efremidis et al., 2001a, b).

Acknowledgements

We gratefully acknowledge financial support of the TMR project CT960062 'Spatio-temporal instabilities in deformation and fracture' of the European Union.

References

Aifantis, E.C. (1996). 'Higher order gradients and size effects'. In: A. Carpinteri (ed.): *Size-scale effects in the failure mechanisms of materials and structures*. London, pp. 231–242.

Aifantis, E.C. (1999a). 'Gradient deformation models at nano, micro, and macro scales'. *ASME Journal of Engineering Materials and Technology* **121**, 189–202.

Aifantis, E.C. (1999b). 'Strain gradient interpretation of size effects'. *International Journal of Fracture* **95**, 299–314.

Altan, B.S. and Aifantis, E.C. (1997). 'On some aspects in the special theory of gradient elasticity'. *Journal of the Mechanical Behavior of Materials* **8**, 231–282.

Altan, S.B. and Aifantis, E.C. (1992). 'On the structure of the mode III crack-tip in gradient elasticity'. *Scripta Metallurgica et Materialia* **26**, 319–324.

Amanatidou, E. and Avras, N. (2002). 'Mixed finite element formulation of strain-gradient elasticity problems'. *Computer Methods in Applied Mechanics and Engineering* **191**, 1723–1751.

Askes, H. (2000). 'Advanced spatial discretisation strategies for localised failure – mesh adaptivity and meshless methods'. Dissertation, Delft University of Technology.

Askes, H. and Metrikine, A.V. (2002). 'One-dimensional dynamically consistent gradient elasticity models derived from a discrete microstructure. Part 2: Static and dynamic response'. *European Journal of Mechanics A/Solids*, 21,573–588.

Askes, H., Pamin, J. and de Borst R. (2000). 'Dispersion analysis and Element-Free Galerkin solutions of second and fourth-order gradient-enhanced damage models'. *International Journal for Numerical Methods in Engineering* **49**, 811–832.

Askes, H., Suiker, A.S.J. and Sluys, L.J. (2001a). 'Dispersion analysis and numerical simulations of second-order and fourth-order strain gradient models based on a microstructure'. In: Z. Waszczyszyn and J. Pamin (eds.), *European Conference on Computational Mechanics*.

Askes, H., Suiker, A.S.J. and Sluys, L.J. (2001b). 'Dispersion analysis and numerical simulations of wave propagation in homogenised granular media'. In: W. Wall, K.-U. Bletzinger, and K. Schweizerhof (eds.), *Trends in Computational Structural Mechanics*. pp. 59–68.

Askes, H., Suiker, A.S.J. and Sluys, L.J. (2002). 'A classification of higher-order strain gradient models–linear analysis'. *Archive of Applied Mechanics*, 72,171–188.

Bažant, Z.P. (1984). 'Size effect in blunt fracture: concrete, rock, metal'. *ASCE Journal of Engineering Mechanics* **110**, 518–535.

Bažant, Z.P. (2000). 'Size effect'. *International Journal of Solids and Structures* **37**, 69–80.

Belytschko, T., Krongauz, Y., Organ, D., Fleming, M. and Krysl, P. (1996). 'Meshless Methods: an overview and recent developments'. *Computer Methods in Applied Mechanics and Engineering* **139**, 3–47.

Belytschko, T., Lu, Y.Y. and Gu, L. (1994). 'Element-free Galerkin methods'. *International Journal for Numerical Methods in Engineering* **37**, 229–256.

Carpinteri, A. (ed.) (1996). *Size-scale effects in the failure mechanisms of materials and structures*. London, E. & F.N. Spon.

Carpinteri, A., Chiaia, B. and Ferro, G. (1995). 'Multifractal sealing law: an extensive application to nominal strength size effect of concrete structures'. Technical Report 51, Politecnico di Torino, Dipartimento di Ingegneria Strutturale.

de Borst, R. and Mühlhaus, H.-B. (1992). 'Gradient-dependent plasticity: formulation and algorithmic aspects'. *International Journal for Numerical Methods in Engineering* **35**, 521–539.

Efremidis, G., Carpinteri, A. and Aifantis, E.C. (2001a). 'Griffith's theory versus gradient elasticity in the evaluation of porous materials tensile strength'. *Journal of the Mechanical Behavior of Materials* **12**, 95–105.

Efremidis, G., Carpinteri, A. and Aifantis, E.C. (2001b). 'Multifractal sealing law versus gradient elasticity in the evaluation of disordered materials compresive strength'. *Journal of the Mechanical Behavior of Materials* **12**, 107–120.

Fleck, N.A., Muller, G.M., Ashby, M.F. and Hutchinson, J.W. (1994). 'Strain gradient plasticity: theory and experiment'. *Acta Metallurgica et Materialia* **42**, 475–487.

Gere, J.M and Timoshenko, S.P. (1991). *Mechanics of Materials*. London: Chapman & Hall, third edition.

Lakes, R.S. (1983). 'Size effects and micromechanics of a porous solid'. *Journal of Materials Science* **18**, 2572–2580.

Lakes, R.S. (1986). 'Experimental microelasticity of two porous solids'. *International Journal of Solids and Structures* **22**, 55–63.

Lu, Y.Y, Belytschko, T. and Gu, L. (1994). 'A new implementation of the element free Galerkin method'. *Computer Methods in Applied Mechanics and Engineering* **113**, 397–414.

Metrikine, A.V. and Askes, H. (2002). 'One-dimensional dynamically consistent gradient elasticity models derived from a discrete microstructure. Part 1: Generic formulation'. *European Journal of Mechanics A/Solids*, 21,555–572.

Morrison, J.L.M. (1939). 'The yield of mild steel with particular reference to the effect of size of specimen'. *Proceedings of the Institute of Mechanical Engineers* **142**, 193–223.

Mûhlhaus, H.-B. and Aifantis, E.C. (1991). 'A variational principle for gradient plasticity'. *International Journal of Solids and Structures* **28**, 845–857.

Pamin, J. (1994). 'Gradient-dependent plasticity in numerical simulation of localization phenomena'. Dissertation, Delft University of Technology.

Pamin, J., Askes, H. and de Borst, R. (1999). 'An element-tree Galerkin method for gradient plasticity'. In: W. Wunderlich (ed.): *European Conference on Computational Mechanics – Solids, Structures and Coupled Problems in engineering*.

Peerlings, R.H.J. (1999). 'Enhanced damage modelling for fracture and fatigue'. Dissertation, Eindhoven University of Technology.

Peerlings, R.H.J., de Borst, R., Brekelmans, W.A.M. and de Vree, J.H.P. (1996a). 'Gradient enhanced damage for quasi-brittle materials'. *International Journal for Numerical Methods in Engineering* **39**, 3391–3403.

Peerlings, R.H.J., de Borst, R., Brekelmans, W.A.M., de Vree, J.H.P. and Spee, I. (1996b). 'Some observations on localisation in non-local and gradient damage models'. *European Journal of Mechanics A/Solids* **15**, 937–953.

Peerlings, R.H.J., de Borst, R., Brekelmans, W.A.M. and Geers, M.G.D. (1998). 'Gradient-enhanced damage modelling of concrete fracture'. *Mechanics of Cohesive-Frictional Materials* **3**, 323–342.

Pijaudier-Cabot, G. and Bažant, Z.P. (1987). 'Nonlocal damage theory'. *ASCE Journal of Engineering Mechanics* **113**, 1512–1533.

Richards, C.W. (1958). 'Effect of size on the yielding of mild steel beams'. *Proceedings of the American Society for Testing and Materials* **58**, 955–970.

Ru, C.Q. and Aifantis, E.C. (1993). 'A simple approach to solve boundary-value problems in gradient elasticity'. *Acta Mechanica* **101**, 59–68.

van Vliet, M.R.A. (2000). 'Size effect in tensile fracture of concrete and rock'. Dissertation, Delft University of Technology.

Vardoulakis, I. and Sulem, J. (1995). *Bifurcation analysis in geomechanics*. London: Blackie Academic and Professional.

Zhu, H.T., Zbib, H.M. and Aifantis, E.C. (1997). 'Strain gradients and continuum modeling of size effect in metal matrix composites'. *Acta Mechanica* **121**, 165–176.

Zienkiewicz, O.C. and Taylor, R.L. (1989). *The finite element method – volume I*. Berkshire: McGraw - Hill, fourth edition.